Bioconjugate Chemistry

pubs.acs.org/bc

Article

# Protein Corona Formation on Lipid Nanoparticles Negatively Affects the NLRP3 Inflammasome Activation

Maharshi Debnath, James Forster, III, Anujan Ramesh, and Ashish Kulkarni*

Cite This: *Bioconjugate Chem.* 2023, 34, 1766−1779

Read Online

ACCESS | Metrics & More | Article Recommendations | Supporting Information



**ABSTRACT:** The interaction between lipid nanoparticles (LNPs) and serum proteins, giving rise to a unique identification in the form of the protein corona, has been shown to be associated with novel recognition by cell receptors. The presence of the corona enveloping the nanoparticle strongly affects the interplay with immune cells. The immune responses mediated by protein corona can affect nanoparticle toxicity and targeting capabilities. But the intracellular signaling of LNPs after corona formation resulting in the change of nanoparticles' ability to provoke immune responses remains unclear. Therefore, a more systematic and delineated approach must be considered to present the correlation between corona complexes and the shift in nanoparticle immunogenicity. Here, we studied and reported the inhibiting effect of the absorbed proteins on the LNPs on the NLRP3 inflammasome activation, a key intracellular protein complex that modulates several inflammatory responses. Ionizable lipid as a component of LNP was observed to play an important role in modulating the activation of NLRP3 inflammasome in serum-free conditions. However, in the presence of serum proteins, the corona layer on LNPs caused a significant reduction in the inflammasome activation. Reduction in the lysosomal rupture after treatment with corona-LNPs significantly reduced inflammasome activation. Furthermore, a strong reduction of cellular uptake in macrophages after the corona formation was observed. On inspecting the uptake mechanisms in macrophages using transport inhibitors, lipid formulation was found to play a critical role in determining the endocytic pathways for the LNPs in macrophages. This study highlights the need to critically analyze the protein interactions with nanomaterials and their concomitant adaptability with immune cells to evaluate nano−bio surfaces and successfully design nanomaterials for biological applications.

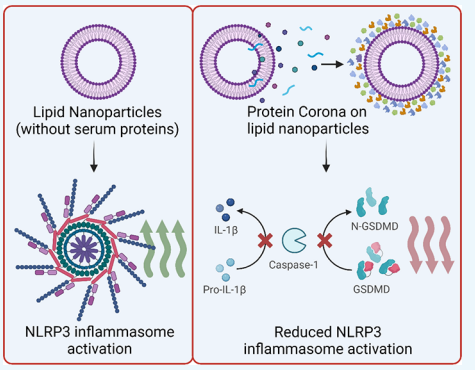


## INTRODUCTION

Recently, lipid nanoparticles (LNPs) have emerged in the pharmaceutical industry as a promising means of delivering a wide range of therapeutics.[1,2] The success of LNPs in providing controlled and targeted drug delivery in specific locations within the body has brought them to the forefront of drug delivery research and development.[3−5] Several formulations of LNPs have been developed for the controlled release of small molecule drugs, siRNA, and mRNA.[3,6,7] However, there are still some challenges associated with using LNPs as drug delivery systems, such as their stability, potential toxicity, and, most importantly, their interaction with the immune system.[8] The undesirable recognition of LNPs by the immune system and subsequent immunotoxicity have been a constant hindrance to their use in clinical trials.[9−12] Thus, controlling the interaction between nanocarriers and immune cells needs to be prioritized for developing an efficient LNP-based drug delivery platform.[13]

Nanoparticles, when in the bloodstream, absorb proteins in the surroundings to form a complex termed protein corona.[9,13] This protein adsorption has been studied and described as a dynamic process where proteins get adsorbed and desorbed depending on their affinities for the nanosurface.[14] Whereas some proteins having high binding energy get adsorbed almost irreversibly, giving rise to the hard corona, some proteins show only a little affinity and stay loosely bound to form the soft corona.[15] Importantly, this phenomenon of protein corona formation controls the toxicity, biodistribution, cellular uptake, and interfacial properties of nanoparticles, thus giving them a distinct biological identity.[16,17] This new identity can affect the nanoparticle−cell interaction by exhibiting novel interactions with cell receptors.[18] The adsorption process is a complex phenomenon that is dependent on several factors. Size, shape, hydrophobicity, and surface charge of the nanoparticles all contribute to the corona composition,[9,19] which eventually determines the ultimate fate of the nanoparticles.[20] In many cases, the protein corona has been found to interact with the immune cells where opsonins like complement proteins,

**Received:** July 21, 2023
**Revised:** September 1, 2023
**Published:** September 14, 2023

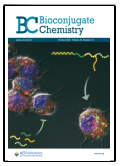





https://doi.org/10.1021/acs.bioconjchem.3c00329
*Bioconjugate Chem.* 2023, 34, 1766−1779

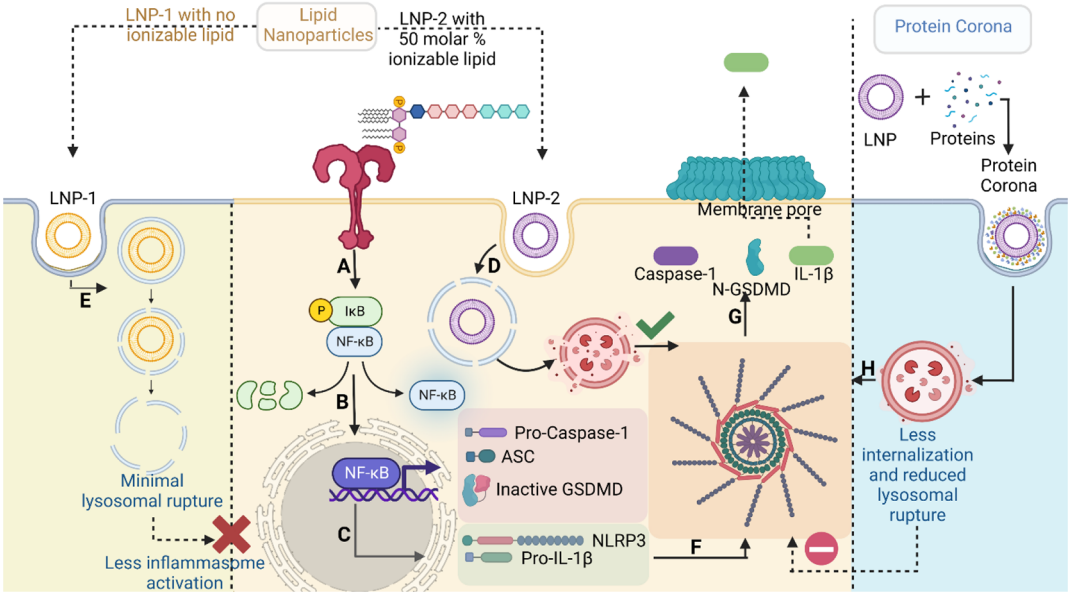


**Figure 1.** Schematic showing the pathway for inflammasome activation by lipid nanoparticles and protein corona. (A) The toll like receptor 4 can recognize lipopolysaccharide to initiate signal-1 and trigger the downstream process to (B) activate NF-KB that causes (C) transcription of inactive inflammasome proteins NLRP3 and pro-IL-1B. Required signal-2 is provided by two lipid nanoparticle formulations shown as LNP1 and LNP2 (D, E) having no ionizable lipid and 50 molar % ionizable lipid, respectively, which depending on the biophysical characteristics will internalize and rupture lysosomal membrane to (F) activate the inflammasome complexation to different extents. This in turn triggers the proteolytic cleavage of pro-caspase-1, pro-IL-1$\beta$, and gasdermin D in their active forms, thus forming pores on the cell surface and finally resulting in cytokine release (G) to cause cell death by pyroptosis. However, protein corona formation results in reduced endocytosis in macrophages and (H) significantly decreased lysosomal rupture. This combined effect causes inflammasome deactivation.

immunoglobulins, and apolipoproteins play an important role in detecting nanoparticles by macrophages.[12] Furthermore, proteins absorbed on the nanosurface can undergo structural changes under the influence of pH.[13] The unfolded protein structure on the corona has been shown to be strongly correlated with the reactive oxygen species (ROS) level and the subsequent activation and deactivation of proinflammatory cytokines.[21] Also, protein corona has been shown to be a key player in modulating macrophage phenotype repolarization.[22] Therefore, there is a crucial need to have a deeper understanding of the possible consequences of protein corona formation on the immune system to design an efficient nanoparticle-based therapeutic agent.

It is also being elucidated that the corona proteins can interact with the innate immune system to regulate cellular stress and damage signals via the regulation of inflammasomes.[23] Here, we tried to conduct a systematic study to find the effect of the protein corona on the NLRP3 inflammasome complex, which gets activated by various stress and damage signals in immune cells.[24,25] The NLRP3 inflammasome is an important target for investigation as several diseases like rheumatoid arthritis, Parkinson's disease, Alzheimer's disease, atherosclerosis, etc., are linked to it.[26] This multimeric protein complex potentially needs two signals for its activation. Signal-1 is called the priming (Figure 1A), where receptors on the surface of macrophages like toll-like receptor 4 (TLR4) can sense lipopolysaccharide (LPS), activating the transcription factor NF$\kappa$B (Figure 1B), which induces the production of inactive proteins like NLRP3 and pro-IL1$\beta$[27,28] (Figure 1C). It is only in the presence of signal-2 (Figure 1D,E), which can be in the form of cellular stress signals, that these inactive proteins oligomerize to form the NLRP3 inflammasome (Figure 1F). Its activation cleaves active caspase-1 and IL-1$\beta$ and allows the GSDMD to promote the release of these proinflammatory cytokines in an immunogenic cell death process called pyroptosis[29,30] (Figure 1G). Although it is well studied that several nanomaterials can nonspecifically activate inflammasome,[31,32] their effective outcome upon corona formation on the inflammasome activation is unknown. An approach is yet to be taken to govern the underlying molecular mechanism of how protein corona affects inflammation. Furthermore, the role of the lipid formulation on the corona composition and its subsequent interaction with immune cells also requires attention.

In this study, we engineered two lipid-based nanoparticle formulations (LNPs) by varying the concentration of each lipid constituent. Experiments were performed to quantify the hard corona proteins in each LNP upon incubation with serum. An extensive study was conducted to investigate the change in the immunogenicity of the LNPs due to the protein adsorption phenomena by measuring the activation of the NLRP3 inflammasome complex in LPS-primed immortalized bone-marrow-derived macrophages (iBMDMs). Interestingly, a suppressed activation of the NLRP3 inflammasome complex was observed upon protein corona formation. We analyzed various pathways and validated the reduced lysosomal rupture (Figure 1H) as the primary reason for the diminished activation of NLRP3 inflammasome. The trend in the observations was confirmed by several experiments involving IL-1$\beta$ release, ASC speck formation, lysosomal rupture, and internalization. The potential mechanisms of cellular uptake of each LNP were also analyzed and compared in the presence and absence of serum proteins. We found a strong involvement of lipid constituents and corona proteins in the endocytic pathway. Overall, the study provides evidence for the potential of protein corona to interfere with innate immune responses


https://doi.org/10.1021/acs.bioconjchem.3c00329
Bioconjugate Chem. 2023, 34, 1766−1779

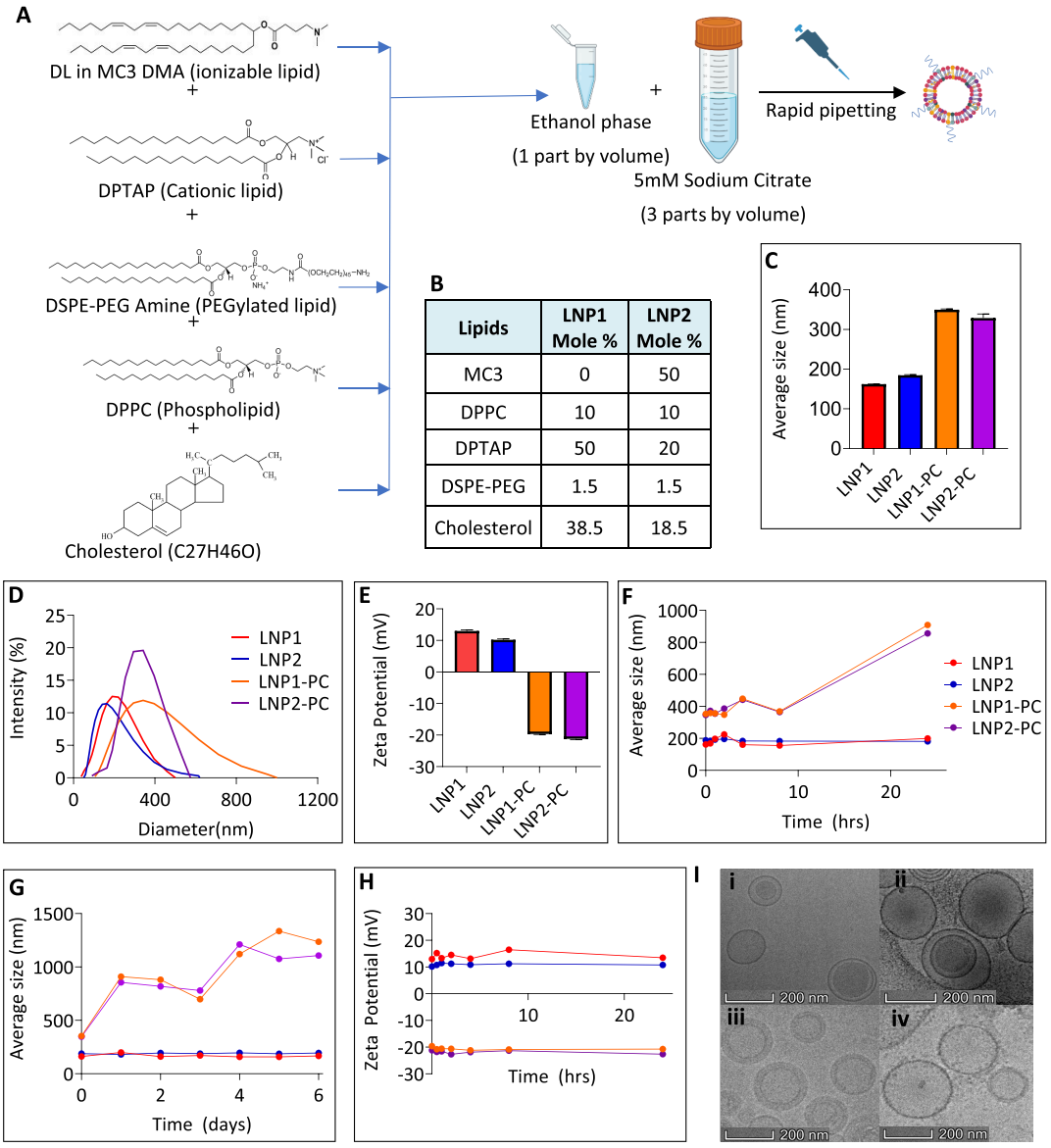


| Lipids | LNP1 Mole % | LNP2 Mole % |
|---|---|---|
| MC3 | 0 | 50 |
| DPPC | 10 | 10 |
| DPTAP | 50 | 20 |
| DSPE-PEG | 1.5 | 1.5 |
| Cholesterol | 38.5 | 18.5 |

**Figure 2.** Synthesis and characterization of two different lipid nanoparticle systems. (A) Schematic of the ethanol dilution method using five different lipids. DL in MC3 DMA (ionizable lipid), DPTAP (cationic lipid), DSPE-PEG amine (PEGylated lipid), DPPC (phospholipid), and cholesterol (C27H46O) are dissolved in ethanol. Sodium citrate buffer (5 mM) is used as the aqueous phase followed by rapid mixing to form the LNPs. (B) Chart showing the molar percentage of each of the different lipids used in the formulation of LNP system. (C) LNP/corona sizes were determined by dynamic light scattering using the intensity Z-average size. Data shown are ±S.E.M. ($n$ = 3). (D) Intensity percent plots for the size of LNP and protein corona. (E) Zeta potential of the LNP/corona as determined by dynamic light scattering. Changes in LNP and protein corona size in PBS over (F) 24 h and (G) 6 days. (H) Changes in the zeta potential for LNP/corona over 24 h. (I) Cryo-TEM images of LNPs with and without corona (i) LNP2, (ii) LNP2-PC, (iii) LNP1, and (iv) LNP1-PC.

actively. A far-reaching implication of the work is expected to aid in determining the appropriate lipid formulation to regulate the corona layer formation and thus achieve a controlled inflammasome activation.

## RESULTS AND DISCUSSIONS

**Synthesis and Characterization of Lipid Nanoparticles with Varying Lipid Compositions for Protein Corona Formation and NLRP3 Inflammasome Exploration.** The protein corona was formed on two different LNP systems, and their effect on NLRP3 inflammasome was analyzed. The two nanoparticles were formed by methodically varying the molar percentage of the five primary lipid constituents: ionizable lipid, cationic lipid, phospholipid, PEGylated lipid, and cholesterol (Figure 2A). 4-(Dimethyl amino)-butanoic acid, (10Z,13Z)-1-(9Z,12Z)-9,12-octadecadien-1-yl-10,13-nonadecadien-1-yl ester (DLin-MC3-DMA), as approved by the US Food and Drug Administration (FDA) for clinical use for small interfering RNA (siRNA) delivery[33,34] and also known to interfere with NLRP3 inflammasome activation,[25] was chosen as the ionizable lipid. 1,2-Dipalmitoyl-3-trimethylammonium-propane chloride (DPTAP), known to enhance loading in the lipid bilayer for drug delivery[35] and also to activate inflammasome,[36] was used as the cationic lipid. Surfactant constituent 1,2-dipalmitoyl-*sn*-*glycero*-3-phosphocholine (DPPC) was picked to be used as the phospholipid. Cholesterol, which contributes to the lipid raft stability and organization,[37] and 1,2-distearoyl-*sn*-*glycero*-3-


https://doi.org/10.1021/acs.bioconjchem.3c00329
Bioconjugate Chem. 2023, 34, 1766−1779

phosphoethanolamine-*N*-[amino(polyethylene glycol)-2000] (DSPE-PEG (2000)-Amine) were used as the other two lipids. The primary rationale behind the lipid formulation was to plump for the two ends of the spectrum to vary the ionizable lipid from 0 molar percent in LNP1 to 50 molar percent in LNP2 (Figure 2B). On the other hand, the cationic lipid concentration varied from 50 to 20 mol % from LNP1 to LNP2 (Figure 2B). All the lipids were dissolved in ethanol, and sodium citrate was used as the aqueous phase to form the LNPs by the ethanol dilution method. Once the nanoparticles were formed, the sizes were confirmed by dynamic light scattering (DLS). The sizes of LNP1 and LNP2 were found to be 162.59 ± 16.6 and 181.2 ± 10.4 nm, respectively (Figure 2C). Both LNP1 and LNP2 were then incubated with rat serum to form their corresponding protein corona. The size of the corona complexes was measured by DLS before isolating the hard corona, which is shown in Figure 2C,D. Interestingly, there is an equivalent negative shift in the zeta potential due to the protein corona formation (Figure 2E). Serum proteins are negatively charged at a pH of 7, and therefore, their accumulation on the LNP surface might cause the zeta potential to decrease.[38] The stability of the LNPs was examined by measuring the changes in size and zeta potential over a period of 6 days (Figure 2F−H). The LNP systems were found to be stable for that period, whereas there was an increase in the size of the corona over time. This can be attributed to the fact that the adsorption equilibrium shifts toward the proteins with high affinities for LNP surface from the initial abundant proteins in the serum,[39] and thus, the unbound or the loosely bound proteins readily detach from the nanoparticle surface, causing aggregation.

**Determination of Hard Corona Composition.** The proteins adsorbed on both nanoparticles were identified and quantified using liquid chromatography−tandem mass spectrometry (LC−MS/MS). The LNP−corona complexes were ultracentrifuged to remove the unbound proteins and obtain the hard corona (HC). The proteins in the HC were then eluted followed by the addition of trypsin to digest them into peptides before analysis (Figure 3A). The proteins were sorted as per the Peptide Spectral Match (PSM) value to calculate the percentage of total bound proteins on the nanoparticle surface.[40] About 170 proteins were identified for LNP1 and LNP2, among which the top 20 most abundant proteins were listed (Figure 3B). They constituted roughly 70% of the total bound proteins. Interestingly, the top 20 most abundant proteins were the same for LNP1 and LNP2, but the order of abundance varied significantly for certain proteins (Figure 3C). The abundances of proteins in LNP1 and LNP2 individually are shown through pictograms (Figure S1). It implies that certain proteins like apolipoproteins and complement proteins are found in abundance in all nanomaterials, but the abundant proteins are not always the same.[13] The difference in the corona composition for the LNPs suggests the possibility of the protein content having an impact on both the mechanisms of internalization[16] and intracellular signaling pathways.[41] Also, the potential of a protein to efficiently get absorbed on the surface of nanoparticles was not found to be dependent on the availability of the proteins in serum. For example, the normal range of complement protein is about 1−2% in rat serum, whereas it formed 7−8% of the total bound proteins in LNP1 and LNP2. On the other hand, albumin in serum proteins constituting about 40% of the total proteins formed only 5−6% of the hard corona. This can be explained by the kinetics of the adsorption process, where both the concentration and the binding energy of a protein−nanoparticle complex determine the affinity of a protein to a nanomaterial.[13] Also, in coherence with previous studies,[42,43] considerably large amounts of complement, apolipoproteins, and immunoglobulins were identified in the corona formed on lipid nanoparticles.

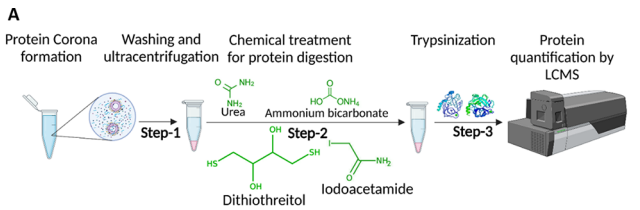


| B Protein | Abundance in LNP1 (%) | Abundance in LNP2 (%) |
|---|---|---|
| Alpha 1 macroglobulin | 12.22 | 9.35 |
| Complement C3 | 7.8 | 7.19 |
| Inter alpha trypsin inhibitor heavy chain H3 | 5.78 | 11.97 |
| Apolipoprotein B100 | 5.62 | 4.11 |
| Albumin | 5.24 | 5.73 |
| Complement C4 | 3.78 | 3.02 |
| Apolipoprotein A1 | 3.9 | 3.85 |
| Murinoglobulin 1 | 3.65 | 3.5 |
| Apolipoprotein E | 3.39 | 3.58 |
| Alpha 1 inhibitor 3 | 3.39 | 3.31 |
| Ceruloplasmin | 2.65 | 3.86 |
| Murinoglobulin 2 | 2.78 | 2.51 |
| Apolipoprotein A4 | 2.1 | 2.15 |
| Complement C9 | 1.43 | 1.43 |
| Fibronectin | 1.36 | 2.04 |
| Complement C5 | 1.19 | 1.16 |
| Prothrombin | 1.11 | 1.15 |
| Serotransferrin | 0.76 | 1.09 |
| Protein AMBP | 1.21 | 1.64 |
| Ig gamma 2A chain C region | 1.48 | 1.28 |
| Others | 29.17 | 26.08 |

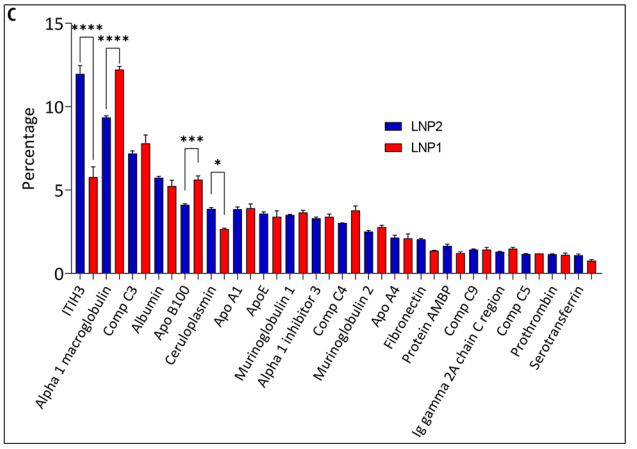


**Figure 3.** Quantification of corona proteins. Relative protein abundance (RPA) of plasma proteins identified in the respective LNPs by quantitative LC−MS/MS. (A) Schematic representation of hard corona quantification. (B) Tabular representation of the 20 most abundant proteins identified in LNP1-PC and LNP2-PC with their percentages. (C) Comparison of the most abundant proteins in LNP1-PC and LNP2-PC. Each value is the average of triplicate ± standard deviation within a single experiment. Statistical analysis was performed with one-way ANOVA followed by Tukey post-test. ns: not significant, *$p < 0.05$, **$p < 0.01$, ****$p < 0.0001$.



https://doi.org/10.1021/acs.bioconjchem.3c00329
Bioconjugate Chem. 2023, 34, 1766−1779

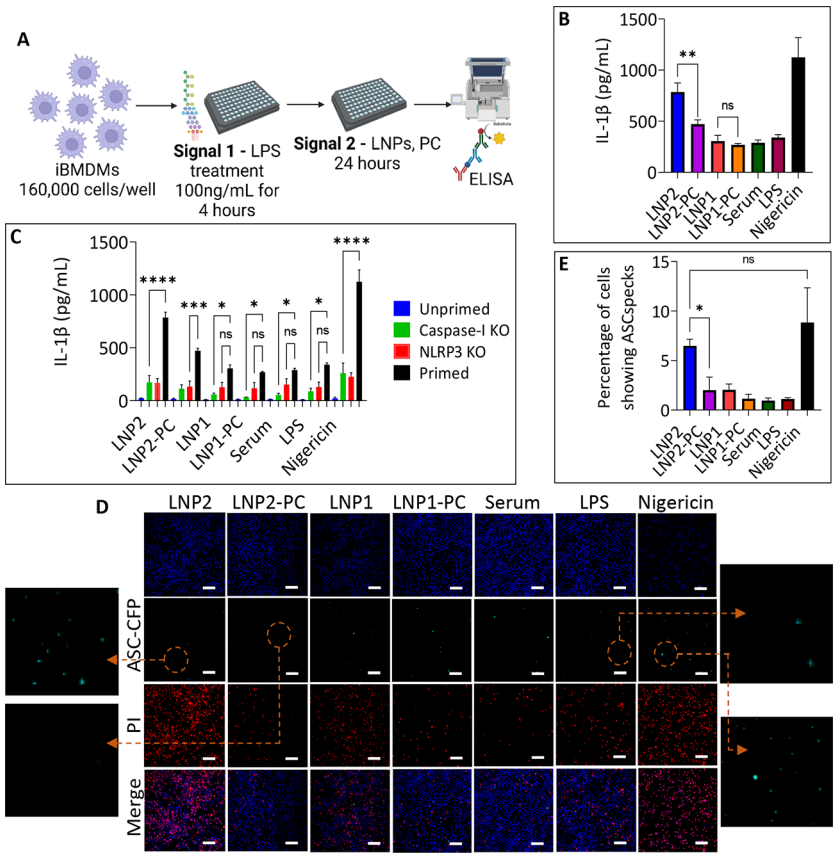


**Figure 4.** LNPs showing different levels of inflammasome activation. Protein corona formation results in a reduction of inflammasome activation for activating LNP. (A) Schematic showing the experiment setup to quantify the inflammasome activation by measuring the release of IL-1B. (B) IL-1$\beta$ release in the supernatant of LPS primed iBMDMs incubated with two different LNPs and their corresponding protein corona for 24 h quantified by ELISA. Data shown are ±S.E.M. ($n$ = 3). Statistical analysis was performed with one-way ANOVA followed by Tukey post-test. ns: not significant, *$p$ < 0.05, **$p$ < 0.01, ****$p$ < 0.0001. (C) We confirmed the involvement of the NLRP3 inflammasome in IL-1$\beta$ release by incubating LNPs with NLRP3 and caspase-1 knockout iBMDMs, as well as iBMDMs unprimed with LPS, showing minimal activation. Data shown are ±S.E.M. ($n$ = 3). Statistical analysis was performed with one-way ANOVA followed by Tukey post-test. ns: not significant, **$p$ < 0.01, ****$p$ < 0.0001. (D) Representative fluorescence microscopy imaging of LPS-primed and LNP treated ASC-CFP expressing iBMDMs stained with NucBlue and PI. Blue fluorescence correlates with stained nuclei by NucBlue, whereas red fluorescence signifies dead cells. Cyan fluorescence correlates with the expression of ASC, where small dots in the sample indicate the formation of ASC specks in the inflammasome complex. Scale bar: 100 $\mu$m. (E) Quantification of ASC specks after 12 h LNP and PC incubation normalized by the total number of live cells counted by the NucBlue signal. Data shown are ±S.E.M. ($n$ = 3). Statistical analysis was performed with one-way ANOVA followed by Tukey post-test. ns: not significant, *$p$ < 0.05.

**Interaction of the Protein Corona with the NLRP3 Inflammasome Complex.** On the basis of previous studies, nanoparticles without protein corona show nonspecific binding to the immune cells in a serum-free environment. But upon the formation of the corona, these nonspecific bindings are minimized because of protein adsorption and instead give rise to specific bindings that are governed by the proteins on the nanoparticle surface.[44,45] Proteins of the hard corona have higher binding energy, and thus, they can have high enough residence time to influence biological interplay. Some proteins can also bind to the nanoparticle surface irreversibly.[46] Corona proteins are capable of inducing the secretion of proinflammatory cytokines like IL-1$\beta$,[23] thus indicating the activation or suppression of inflammasome. In this study, we have explored the role of protein corona on NLRP3 inflammasome complex by quantifying the IL-1$\beta$ release, which directly correlates to inflammasome activation (Figure 4A). First, the IL-1$\beta$ concentration from LPS primed cells was measured upon 24 h of incubation with pristine nanoparticles at a concentration of 200 $\mu$g/mL of total lipids in serum-free media (Figure 4B). Nigericin, which is a strong signal-2 provider for NLRP3 inflammasome activation,[47] at a concentration of 10 $\mu$M was used as a positive control for the IL-1$\beta$ study. In accordance with previous findings,[25,48,49] the nanoparticle with higher ionizable lipids was found to significantly result in IL-1$\beta$ secretion, whereas the one with no ionizable lipid showed minimal IL-1$\beta$ secretion. Next, we wanted to explore how protein adsorption affects nanoparticle interaction with macrophages. As recent studies[18,50,51] demonstrate the protein corona to be a complex that gives an entirely new identity to the nanoparticle resulting in the loss of targeting characteristics, thus affecting both the pharmacokinetics and stability of a nanocarrier, we hypothesized that the shielding effect by the proteins could have an obstructing role in NLRP3 inflammasome activation. To investigate this, LPS-primed iBMDMs were used as an in vitro model. After treating the cells with 100 ng/mL of LPS for 4 h to effectively provide signal-1, the cells were incubated with LNPs and their corona complex at the same concentration of 200 $\mu$g/mL. The supernatants were collected after 24 h and tested for IL-1$\beta$ concentration by an enzyme-linked immunosorbent assay (ELISA). We observed that protein corona formation results


https://doi.org/10.1021/acs.bioconjchem.3c00329
Bioconjugate Chem. 2023, 34, 1766−1779

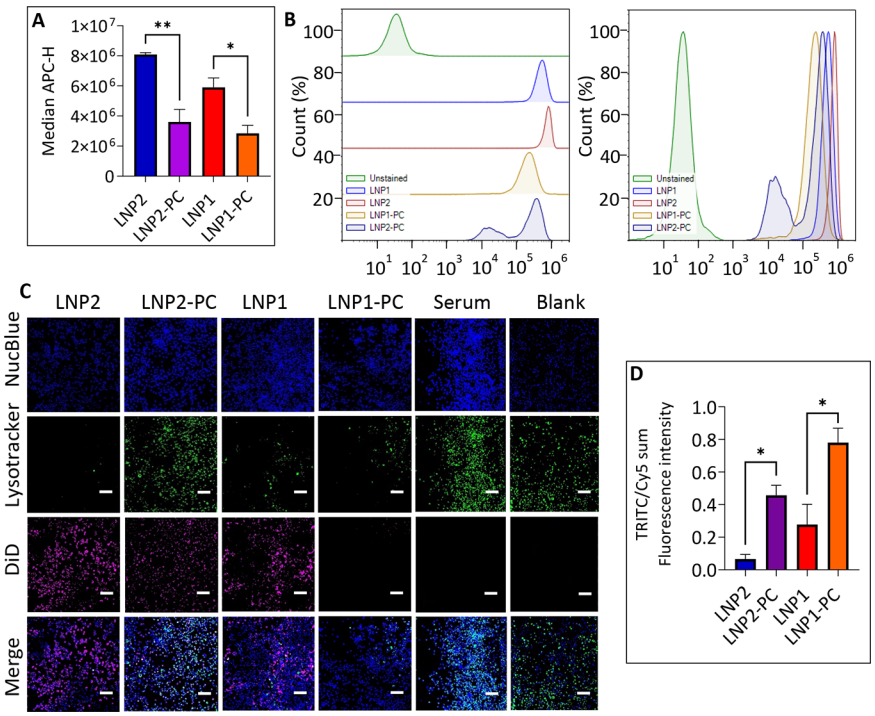


**Figure 5.** Protein corona reduces internalization and lysosomal rupture. (A) LNP internalization was determined by incubating DiD-loaded LNPs in CFSE-stained iBMDMs at 37 °C and analyzing the number of CFSE-positive events expressing APC signal and DiD positive cells indicating internalization of DiDloaded LNPs using flow cytometry. Data shown are ±S.E.M. ($n$ = 3). (B) Relative and superimposed internalization of LNPs and protein corona in iBMDMs from flow cytometry. (C) Representative fluorescence microscopy imaging of iBMDMs treated with DiD-encapsulating LNPs for 4 h and stained with NucBlue and Lysotracker Red DND-99. Blue fluorescence correlates with stained nuclei by NucBlue, green fluorescence signifies lysosomes, and pink fluorescence signifies internalized DiD-LNPs. Scale bar: 100 $\mu$m. (D) Quantification of lysosomal fluorescence intensity normalized by internalized DiD particles quantified by Cy5 fluorescence. Data shown are ±S.E.M. ($n$ = 3).

in a reduction of NLRP3 inflammasome activation (Figure 4B). This effect was found to be more prominent for LNP2 (1.7-fold reduction), which can potently cause NLRP3 inflammasome activation in serum-free media. Next, we wanted to inspect the NLRP3 oligomerization leading to caspase 1 activation and, thus, the involvement of NLRP3 and caspase 1 protein in the signaling pathway causing IL-1$\beta$ secretion. To examine this, cells that were knocked out for either NLRP3 or caspase 1 were incubated with the same nanoparticles with and without corona, and the IL-1$\beta$ release from the supernatant was quantified by ELISA. LPS unprimed iBMDMs were also treated with LNPs with and without corona. On comparing the IL-1$\beta$ release from these control groups with respect to WT iBMDMs, a significant decrease in the concentration of IL-1$\beta$ was noticed (Figure 4C), thus affirming the association of these proteins in the cell signaling pathway.

To gain further mechanistic insights, we visualized the effect of corona formation on the complexation of NLRP3 inflammasome proteins. We imaged and quantified the adaptor protein ASC (apoptosis-associated speck-like protein containing a CARD) speck formation in iBMDMs engineered to express CFP-tagged ASC protein upon exposure to signal-1 and -2 required for NLRP3 inflammasome activation. ASC proteins are generally dispersed inside the cytosol. However, during the inflammasome activation, the ASC acts by bridging NLRP3 proteins with pro-caspase 1 within the inflammasome complex, eventually resulting in caspase 1 maturation and IL-1$\beta$ secretion.[52,53] These conformational changes nucleate the formation of large cytosolic aggregates called ASC specks. These specks can form a platform to recruit procaspase-1, thus activating caspase-1 and the maturation of IL-1$\beta$.[54] As the ASC speck assembly and the NLRP3 inflammasome activation are concomitant events,[55] ASC speck formation can be used as a simple upstream readout for inflammasome activation. To explore this visually, cells were first primed with TLR4 grade LPS and then incubated with DiD-tagged LNPs with and without serum proteins for 13 h. The cells were stained with NucBlue and propidium iodide (PI) and imaged using a CREST v2 confocal light microscope. Fluorescence microscopic images revealed minimal ASC speck formation (CFP channel) and cell death (PI channel) for just the LPS primed groups and the serum-added groups (Figure 4D). This minimal speck formation indicated the ASC proteins being dispersed in the cytosol and thus correlated with no inflammasome activation. Significantly more ASC specks and cell death in LNP2 compared to LNP1 were witnessed, which were congruent to our study of IL-1$\beta$ secretion using ELISA resulting in higher inflammasome activation by LNP2. Now, upon the formation of the protein corona on LNPs, a significant reduction of ASC specks (3.25-fold for LNP2 and 1.8-fold for LNP1) normalized by the total number of cells (Figure 4E) as well as lesser cell death by pyroptosis was found when compared with pristine LNPs without any serum proteins. This further corroborates our previous findings by exhibiting a significant decrease in NLRP3 inflammasome activation due to the protein−nanoparticle complex. These findings indicate a negative correlation between the protein corona formation and NLRP3 inflammasome assembly. To further explore the corona interactions, we were prompted to


https://doi.org/10.1021/acs.bioconjchem.3c00329
Bioconjugate Chem. 2023, 34, 1766−1779

conduct a comprehensive study about the mechanisms that led to these observed effects on the NLRP3 inflammasome.

**Cellular Uptake and Lysosomal Rupture Are the Fundamental Mechanisms of Protein-Corona-Induced Suppression of NLRP3 Inflammasome.** Recent studies have demonstrated the dynamic nature of protein corona and how it can evolve over time to significantly influence biological outcomes like cellular uptake by macrophages.[56,57] The interaction of a macrophage with lipids dictates particle clearance. Upon the formation of the corona layer, the adsorbed proteins can modulate the uptake and toxicity of nanoparticles.[58] For example, immunoglobulins form a significant part of the corona, and their deposition on nanoparticle surfaces can influence complement opsonization of lipid nanoparticles.[59] As corona proteins can regulate the uptake of nanoparticles through the recognition by cell receptors,[16] we intended to conduct an internalization study of the lipid nanoparticles in the absence and presence of serum proteins in iBMDMs. As a first step, we incubated carboxyfluorescein *N*-succinimidyl ester (CFSE) stained iBMDMs with 200 $\mu$g/mL of the LNP formulations encapsulating 3 mol % DiD dye in the absence of serum proteins to gauge the fluorescence intensity using flow cytometry and quantify their internalization. Interestingly, a remarkable difference in the cellular uptake was noticed for both the LNPs. In the absence of any corona, LNP2 showed a higher (1.4-fold) internalization than LNP1. This could be due to the high content of the ionizable lipid, which can foster electrostatic attraction and promote nonspecific binding with the negatively charged cell membrane. One of the possible explanations for the higher internalization of LNP2 as compared to LNP1 could be the higher content of ionizable and cationic lipid that can promote electrostatic attraction with the cell membrane and cause increased cellular uptake. However, it is the combined effect of each lipid constituent that determines the LNP characteristics including cellular uptake and the activation of NLRP3 inflammasome in a lysosome-dependent manner. It is worth noting that the protein corona formation caused a significant reduction in the internalization (Figure 5A−C) for both LNP1 (2.15-fold) and LNP2 (2.25-fold). Our results suggest that the corona proteins can shield the nanoparticle−cell interactions with the possibility of losing the specificity and thus their ability to get internalized. However, as less internalization has not always been found directly corresponding to inflammasome activation,[25] we wanted to explore specific mechanisms besides the dwindling cellular uptake of protein corona complexes that result in the NLRP3 inflammasome suppression.

NLRP3 inflammasome can be activated by a wide range of stimuli after LPS priming, including mitochondrial reactive oxygen species (ROS), calcium and potassium ion influx, and lysosomal damage.[27] First, we accessed the $Ca^{2+}$ ion influx in iBMDMs treated with LNPs and protein corona compared to just LPS-primed iBMDMs. To measure the intracellular $Ca^{2+}$ levels, we stained the treated cells with a calcium marker, Fluo-4AM,[60] and quantified the fluorescence intensity by flow cytometry (Figure S2). To test for mitochondrial ROS, we stained the cells with MitoSOX, a widely used staining technique to determine cellular ROS,[61] and analyzed them similarly using flow cytometry (Figure S3). We found that for both the pristine and protein corona coated LNPs, the fluorescence intensity was comparable with just the LPS-primed iBMDMs. Also, corona formation did not significantly change the ROS production or the ion influx after treatment with both LNP1 and LNP2. We did not see any specific trend from Fluo-4 AM and MitoSOX staining, and thus, our observations indicated that $Ca^{2+}$ influx and mitochondrial ROS might not be the governing mechanisms for the LNP-based NLRP3 inflammasome activation and its subsequent suppression upon protein corona formation. The lysosomal rupture was investigated as a next step, which is a key driving force for NLRP3 inflammasome activation via cathepsin-B maturation.[30,62] Following lysosomal membrane damage, the release of lysosomal cathepsin proteins in the cytosol is suggested to be indicative of NLRP3 inflammasome activation[63] Also, the extent of lysosomal rupture has shown to be a regulator of the inflammasome activation, where partial rupture can activate the complex leading to apoptosis but complete rupture or permeabilization can inhibit the activation.[54,64] To evaluate lysosomal damage, the LPS primed iBMDMs were treated with 3 mol % of DiD dye encapsulating LNPs and their coronas for 4 h. The far-red fluorescent lipophilic DiD dye was used to track the internalization of the LNPs in cells. The cells were stained with NucBlue and Lysotracker Red DND-99 before imaging them in CREST v2 confocal fluorescence microscopy. The NucBlue stains the alive cells, and the Lysotracker is widely used in cell biology to stain the lysosomes of the viable cells.[65] It is an acidotropic dye that stains acidic compartments in the cell, and it is specific to lysosomal pH of 4.5−5. Visually, a lower Lysotracker fluorescence intensity was observed for LNP2 (4.21-fold) as compared to LNP1, suggesting greater lysosomal rupture caused by LNP2 resulting in higher NLRP3 inflammasome activation (Figure 5D,E). Also, LNP2 showed higher internalization than LNP1, which was in consistence with our cellular uptake studies by flow cytometry. We also noticed a sequential trend of internalization as well as the lysosomal rupture on comparing the LNPs in the presence and absence of corona proteins. The LNP ingenuity to efficiently rupture the lysosome was found to get reduced significantly upon corona formation in iBMDMs. This is shown by the bright green fluorescence intensity in LNP-PC groups suggesting the existence of intact lysosome (Figure 5D). Serum proteins just by themselves did not cause any lysosomal rupture. Also, just the LPS primed cells showed maximum fluorescence intensity and thus the least lysosomal rupture. Upon measuring the Lysotracker intensity (TRITC channel) normalized with the DiD intensity (Cy5 channel) that corresponds to internalization, the effective lysosomal damage (Figure 5E) was plotted. On calculating the Pearson coefficient ($r$) for each group, we found a minimal dependency between lysosomal rupture and internalization for LNP2, whereas LNP1, LNP1-PC, and LNP2-PC have been found to have a strong correlation between the two factors. This suggests to the fact that at a diminished uptake in macrophages, the internalization might be the determining factor to estimate the lysosomal rupture. Here, we were able to quantify the Lysotracker signal with and without the protein corona formation that effectively lowered the ability of both the LNPs to cause lysosomal permeabilization (2.8- and 6.93-fold decrease for LNP1 and LNP2, respectively). These studies collectively indicate that the corona adsorption on nanoparticles negatively correlates with the NLRP3 inflammasome. Moreover, the shielding effect of adsorbed proteins resulting in inefficient cellular uptake and minimized lysosomal rupture is the primary mechanism for the observed inhibiting effect.


https://doi.org/10.1021/acs.bioconjchem.3c00329
Bioconjugate Chem. 2023, 34, 1766−1779

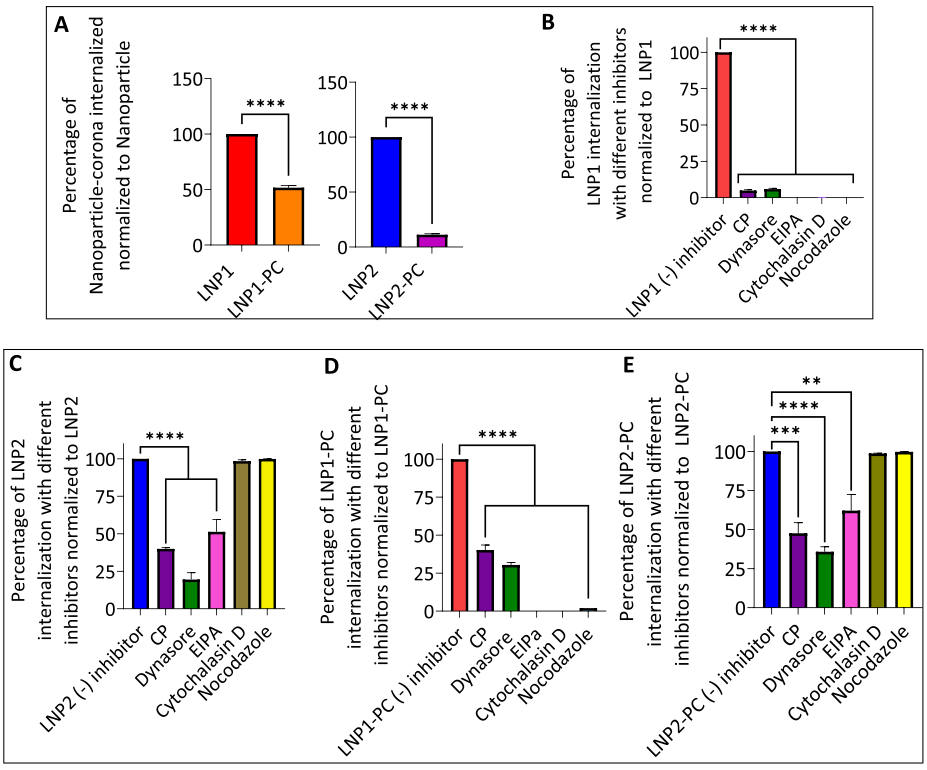


**Figure 6.** Characterization of uptake mechanism of the corona formed on lipid nanoparticles. The protein corona−nanoparticles formed were added to $10^6$ iBMDMs at a final concentration of 200 $\mu$g/mL in either the absence or presence of 100 $\mu$M EIPA, 10 $\mu$g/mL chlorpromazine (CP), 25 $\mu$g/mL Dynasore (D), 2.5 $\mu$g/mL cytochalasin D (C), or 5 $\mu$M nocodazole (N). Uptake extents were obtained by flow cytometry. (A) Percentage of nanoparticles−corona internalized in the absence of any inhibitor for both LNP1 and LNP2 normalized to the raw nanoparticles without any serum proteins. Percentage of LNP1(B.1), LNP2 (B.2), LNP1-PC (B.3), and LNP2-PC (B.4) getting internalized by iBMDMs with the various inhibitors one at a time at the mentioned concentrations normalized with respect to the internalization without any inhibitor. Each value is the average of triplicates ± standard deviation within a single experiment. Statistical analysis was performed with one-way ANOVA followed by Tukey post-test. ns: not significant, *$p < 0.05$, **$p < 0.01$, ****$p < 0.0001$.

**Evaluation of Cellular Uptake of LNPs with and without Protein Corona.** Macrophages are the first line of defense[66] against pathogens. They are phagocytic cells that are built to ingest and destroy all foreign invaders in a generalized way without any specific individuals.[67] Macrophages have developed several techniques to internalize nanoparticles including phagocytosis, receptor-mediated endocytosis, and pinocytosis.[68] Previous studies suggested that protein corona formation can hinder particle recognition by macrophages.[69] Thus, a mechanistic approach to studying the factors that determine the endocytic pathway, including LNP formulation as well as the multilayered corona composition, is a key step to answer questions relating to circulation time, biodistribution, toxicity, and most notably the particle interaction with the immune system, for example, the activation/deactivation of the NLRP3 inflammasome complex. To study the functional changes due to the corona formation and to characterize the uptake mechanisms of LNPs in the presence and absence of serum proteins, we used different endocytosis inhibitors, each corresponding to a specific pathway.[16,70] Chlorpromazine hydrochloride, a cationic amphiphilic drug, was used to inhibit clathrin-mediated endocytosis. It functions by inhibiting AP2, a key adaptor protein that otherwise can simultaneously bind to clathrin and membrane proteins, thereby directing the assembly of a clathrin coat around the cargo that is destined to be internalized.[71−73] Dynasore, an inhibitor of dynamin GTPase activity, prevents the hydrolysis of dynamin-bound GTP, thus restricting the conformational changes that result in pinching off the clathrin/AP-coated vesicle bud in cytosol.[74] EIPA (5-*N*-ethyl-*N*-isopropyl amiloride) was used to obstruct micropinocytosis. It functions by impeding the $Na^+/H^+$ exchange, thus lowering the submembranous pH.[75] Finally, cytochalasin D and nocodazole were used to inhibit actin and microtubule-dependent endocytosis. They disrupt the cytoskeleton by binding to the actins and microtubules, thus hindering both actin polymerization and elongation.[16,76]

The efficacy of the inhibitors was accessed in both the presence and absence of serum proteins. First, the iBMDMs were stained with CD45 antibody without any inhibitors and checked for double positivity for DiD encapsulating dye using flow cytometry (Figure 6A). Two- and 10-fold decreases in cellular uptake for LNP1-protein corona and LNP2-protein corona were observed, respectively. Next, cells were treated with all the inhibitors at a fixed concentration, one at a time for each of the four groups (LNP1, LNP1-PC, LNP2, and LNP2-PC). For LNP1, all the inhibitors were effectively causing efficient inhibition of internalization, with EIPA, cytochalasin D, and nocodazole being the most potent, resulting in complete inhibition (Figure 6B). For LNP2, Dynasore was the most effective inhibitor, causing a 5-fold reduction in cellular uptake, followed by chlorpromazine hydrochloride and EIPA, which showed around 50% inhibition (Figure 6C). These specific inhibitors would suggest a more predominant endosome mediated uptake in macrophages for LNP2 unlike in LNP1 where multiple endocytic pathways are involved. And this would directly correlate with LNP2 following the


https://doi.org/10.1021/acs.bioconjchem.3c00329
Bioconjugate Chem. 2023, 34, 1766−1779

endolysosomal pathway and eventually end up in the lysosomal compartment, thus causing the maximum disruption. Thus, this study with the inhibitors aligns with the previous findings of LNP2 causing the highest lysosomal rupture for inflammasome activation. Surprisingly, cytochalasin D and nocodazole showed no reduction, suggesting the nonalignment of actin and microtubules-dependent endocytosis for LNP2. Next, the efficacy of the inhibitors was quantified after corona formation. To compare the potency of the inhibitors with corona proteins for both the LNP formulations, the protein corona groups without inhibitors were considered as absolute values, i.e., totally internalized, and the groups with corona along with inhibitors were normalized with respect to that. Here, we observed that for LNP1-PC, the cellular uptake showed a 2.5-fold reduction for chlorpromazine hydrochloride compared to 20-fold in the case of pristine LNP1 without serum proteins. Also, for Dynasore, we reported 3.5-fold inhibition compared to 16-fold for LNP1 in the absence of corona proteins. However, EIPA, cytochalasin D, and nocodazole showed complete inhibition of corona complex (Figure 6D). In the case of LNP2-PC, the corona formation did not affect the functionality of the inhibitors significantly. Dynasore showed 2.5-fold reduction as compared to 5-fold for pure LNP2 without corona proteins, whereas cytochalasin D and nocodazole still exhibited no inhibition (Figure 6E). Dynasore and chlorpromazine hydrochloride remain the most potent inhibitors for LNP2-PC, which are similar to what have been observed for LNP2 without serum proteins. This indicates that LNP2-PC would also end up in the endosome but cannot effectively cause the lysosomal damage. This is an interesting finding that sheds light on the possibility of protein corona's composition that could be influencing the nanoparticle's intracellular trafficking and fate. Overall, the results suggest the involvement of multiple pathways of internalization for LNPs in macrophages. Also, the lipid constituents play a vital role in determining the potential endocytic mechanism. Moreover, the corona formation altered the LNP recognition by cell receptors, thus affecting the internalizing pathway. In summary, although a direct correlation between protein corona and endocytic mechanisms might present complexities, it is reasonable to conclude that the presence of a protein corona can influence how endocytic inhibitors interact with nanoparticles and cells. The inhibitors might not act as efficiently on nanoparticles with a protein corona as they do on bare lipid nanoparticles because of the altered nanoparticle−cell interactions brought about by the protein corona.

## CONCLUSIONS

The protein−nanomaterial interactions have been at the forefront of biological immune response therapy. Explaining this inevitable protein adsorption to control immune responses is a fundamental challenge. Our work aimed to elucidate the association between corona−nanoparticle complexes and innate immune responses in macrophages to understand and analyze the effects of protein corona formation on lipid nanoparticles in relation to the NLRP3 inflammasome. Here, we sought to describe the shift in the immunogenicity of lipid nanoparticles due to corona formation to efficiently cause activation of the NLRP3 inflammasome multimeric complex that triggers the release of proinflammatory cytokines like IL-1$\beta$ and IL18, eventually leading to cell death.

The study was designed by characterizing and synthesizing two different LNP formulations. Similar formulations of LNPs have been previously reported to be involved in mRNA delivery.[3] The concept behind the lipid formulation was to maximize the difference in the ionizable lipid content (DLin-MC3-DMA), which has been shown previously to interfere with the NLRP3 inflammasome pathway.[25,77] Several cell-based assays were performed on the two formulations to realize that LNP2, having 50 molar percent of ionizable lipid, can significantly activate the NLRP3 inflammasome complex. At the same time, the activation was minimal for LNP1, which has no ionizable lipid. But when the corona layer was formed on the surface of the LNPs, a significant reduction in the NLRP3 inflammasome activation was observed. It is worth mentioning that only certain specific proteins formed the significant component of the corona for the LNP formulations. This finding aligns with a study conducted by Walkey and Chan,[13] where a similar abundance of a few distinct proteins was observed on a panel of 63 different nanomaterials. A systematic approach to the study helped us to uncover the underlying mechanism for the inhibiting effect of the corona layer. Mechanistic cell-based assays revealed the role and reciprocity of multiple signaling cascades toward regulating the NLRP3 inflammasome activation by protein corona. The reduced lysosomal disruption by the corona as compared to pristine LNPs was reported as the primary cause of the corona-based NLRP3 inflammasome suppression. Our study displayed a significant decrease in the lysosomal rupture due to the shedding effect of the corona complex. One possible explanation for this is the intracellular fate of the protein corona, which is different from pristine LNPs. Whereas LNPs are most likely to follow the canonical endolysosomal pathway, which may result in the collapse of lysosomal homeostasis depending on their ability to undergo endosomal escape, corona-coated LNPs, after internalization, can get translocated to the cytosol or other compartments outside the endolysosomal system. This was explained by Han et al.,[78] who exhibited that protein-corona-coated nanoparticles can get redistributed and sorted inside the endosome, indicating the possibility of forming two distinctly loaded endosomal vesicles, each ultimately turning up in different compartments.

Not only the protein coating decides the fate of LNPs once inside the cell. Our observations suggest the involvement of protein corona in the very first interaction between nanoparticles and macrophages. The findings described the mechanism of internalization followed by the nanoparticles in the absence and presence of corona. Different mechanisms were observed for cellular uptake for the two formulations while in serum-free media. But a very significant decrease in cellular uptake was found in the presence of serum proteins, which is in accordance with previous studies[16,79] where the internalization was found to be minimized by the corona. Furthermore, the inhibitor study also suggested that the corona proteins on the surface of the nanomaterial can alter the cell uptake mechanism. These distinct endocytic pathways can be attributed to the various lipid formulations and the corona compositions, which can be further explained by the recognition of corona proteins by the cell receptors that regulate the endocytic pathway for internalization.[16,45,64] Similar results were reported by Francia et al.,[16] where unique mechanisms of internalization were linked with diverse corona composition even for the same nanoparticle. A further extension of our findings can have potential implications in modeling and speculating in vivo conditions where there is an excess of the free unbound protein, which can also contribute


https://doi.org/10.1021/acs.bioconjchem.3c00329
Bioconjugate Chem. 2023, 34, 1766−1779

to the observed mechanisms as reported by Lara et al.,[80] where the free proteins can potentially compete with the corona proteins for the same receptors. However, the total protein concentration, corona composition, and nanoparticle stability can also contribute to the cell−nanoparticle interaction and should also be considered.

Overall, our study provides novel insights into the interplay between protein corona and NLRP3 inflammasome activation. It highlights the ability of the protein corona to be influential in both surface interactions and intracellular signaling pathways. Although we could establish a potential role of lipid formulations, corona formation, and the mechanism for inflammasome suppression, it is possible that the corona can also affect other immune responses like the complement pathway and adaptive immunity. Further studies are required to fully characterize the implications of protein corona in biologically relevant conditions. Although the composition of hard corona significantly contributes to immune cell signaling pathways, there is a need for more detailed information about the soft corona composition, organization, and dynamics to demonstrate such effects linked to individual corona proteins fully. Nevertheless, the reported findings from the study are alluring in a way to realize that this inevitable protein layer formation can have a profound connection with the immune system, explicitly affecting inflammasome activation in innate immune cells. This research indicates that exploiting protein corona can be utilized to regulate inflammasome activation, and it can have immense implications in the field of nanomaterial-based drug delivery.

## METHODS

**Synthesis and Characterization of Lipid Nanoparticles (LNPs).** Five different lipids were used to synthesize the lipid nanoparticles. Stock solutions of DLin-MC3-DMA (ionizable lipid), DPTAP (cationic lipid), DPPC (phospholipid), DSPE-PEG (2000)-Amine (PEGylated lipid), and cholesterol were made in molecular biology grade ethanol. The DPTAP stock solution was sonicated at 37 °C for 30 s to ensure homogeneous mixing in the ethanol phase. Two different systems of LNPs were synthesized via the ethanol dilution method by adding different volumes of each lipid from the stock concentration at the desired molar concentration. The ethanol−lipid mixture was then added dropwise to a 5 mM sodium citrate buffer solution at a 1:3 vol/vol ratio of the ethanol to the aqueous phase followed by rapid pipetting for a minute to form the lipid nanoparticles finally. The final concentration of the LNPs formed was 1.8 mg/mL for both LNP1 and LNP2. For microscopy imaging and flow cytometry studies, 3 molar % DiD dye was used along with the ethanol−lipid mixtures as discussed above. However, for the cellular uptake studies using different endocytosis inhibitors, 0.3 molar % DiD dye was similarly encapsulated in the LNPs. Finally, the LNPs were stored at 4 °C.

**Protein Corona Formation and Characterization.** Corona nanoparticle complexes were formed before incubation on cells. Total proteins from a stock of rat serum were quantified by using a Pierce BCA Protein Assay Kit (Thermo Scientific). LNPs (100 μL) were added to the required volume of rat serum to a final w/w ratio of 1:5 lipids to serum proteins at 37 °C and kept under constant shaking (100 rpm) for 2 h to form the protein corona complexes. To distinguish between the hard and soft corona, the lipid−nanoparticle corona mixtures were centrifuged at 15,000*g* for 15 min to remove the unbound/loosely bound (soft corona) proteins. The pellet was resuspended in PBS and washed three times to obtain the hard corona. For cell experiments, ultracentrifugation was not performed, and the corona complexes were diluted in basal media to a final lipid concentration of 200 μg/mL and then added to cells. The bound proteins were removed from the hard corona complexes for mass spectroscopy analysis. A concentrated 4× Laemmli reducing sample buffer was added to the pellet to elute the proteins from the hard corona-nanoparticles. The reducing buffer has beta-mercaptoethanol, which can strip off the proteins by denaturing them and through the cleavage of the disulfide bonds. For sodium dodecyl-sulfate polyacrylamide gel electrophoresis (SDS-PAGE), the samples were boiled at 95 °C for 5 min after treatment with the reducing buffer. After the electrophoretic run, the gel was incubated with a solution of 0.2% w/v Coomassie blue in methanol/water/glacial acetic acid ratio of 4:5:1 for 2 h with slight shaking (70 rpm), after which it was left in 4:5 methanol/water solution overnight to prepare the final gel for imaging.

**LNP Size Characterization.** The size of the lipid nanoparticles and the corona complexes was determined by dynamic light scattering (DLS) using a Malvern Nanozetasizer ZS90. The sample (10 μL) was diluted in 990 μL of 1× milli-Q. The 1 mL solution was vortexed and then added to disposable sizing cuvettes for size characterization. The average particle sizes were determined by the intensity *Z*-average size, and the intensity stats table was used to plot the sizes.

**Zeta Potential.** For the zeta potential readings, 10 μL of the LNP and corona samples was diluted in 990 μL of 1× milli-Q. The 1 mL solution was then injected into disposable folded zeta cells using a syringe carefully to avoid the formation of bubbles. It was then appropriately placed inside the holder of the Nanozetasizer, and the data were collected using a Malvern Zetasizer instrument.

**Lipid−Nanoparticle Stability.** The size of the lipid nanoparticles and protein corona complexes was measured as discussed before using a Malvern Nanozetasizer at different time intervals of 0 h, 30 min, 1 h, 2 h, 4 h, 8 h, and 24 h. Also, a weekly basis study was obtained by measuring the size of the LNPs and the corona over a period of 7 days. The intensity *Z*-average size was used to measure the sizes. The particles and the corona complexes were stored at 4 °C during the stability studies.

**Procedure for Culturing the Cells Used in the Study.** Engineered immortalized bone-marrow-derived macrophages (iBMDMs) expressing ASC-CFP protein were used in all in vitro experiments. Caspase-1 KO and NLRP3 KO iBMDMs cell lines were used for the knockout IL-1β expression study. ASC-CFP tagged iBMDMs were acquired as a present from Dr. Kate Fitzgerald from the University of Massachusetts Chan Medical School. And the knockout cell lines were obtained from Dr. Fitzgerald. Dulbecco's modified Eagle's medium (DMEM) supplemented with 10% v/v fetal bovine serum (FBS), 0.5% v/v penicillin (50 μg/mL), and 0.5% v/v streptomycin (50 μg/mL) was used as the medium for the cell culture. Also, the medium was refreshed every 48 h. The cells were cultured in T-75 cell culture flasks and were usually split using 0.25% trypsin−EDTA in 1× phosphate-buffered saline (PBS) in a 1/5 reseeding ratio every 2 to 3 days. For accessing inflammasome activation in the cells, the cells were first treated with 100 ng/mL ultrapure lipopolysaccharide (LPS) for 4 h to provide signal-1 priming required for NLRP3


https://doi.org/10.1021/acs.bioconjchem.3c00329
Bioconjugate Chem. 2023, 34, 1766−1779

inflammasome activation. Signal-2 was provided by incubating the LPS-primed iBMDMs with nanoparticles or the protein corona complexes for 24 h at a final 200 $\mu$g/mL lipid concentration. For cell uptake studies, cells were incubated with LNPs/corona complexes and specified concentrations of different inhibitors for 30 min, 1 h, and 2 h to study the extent of nanoparticles internalizing the cells.

**IL-1$\beta$ ELISA.** iBMDMs were seeded in a 96-well plate, and the ELISA was started at a density of 160,000 cells per well. First, the cells were primed with 100 ng/mL of ultrapure LPS for 4 h for the signal-1 required for inflammasome activation. Two LNP systems and their corresponding corona complexes were added at a final 200 $\mu$g/mL lipid concentration for 24 h. LPS primed iBMDMs with no signal-2 were used as a negative control, and primed cells with nigericin at a concentration of 1 $\mu$L/mL was a positive control. The supernatant from the cells was collected to measure the concentration of IL-1$\beta$ by performing ELISA using the Invitrogen Mouse IL-1$\beta$ ELISA kit as recommended in the manufacturer's protocols.

**Confocal Microscopy for ASC Speck Imaging.** iBMDMs were seeded in eight-well glass chamber slides a day or two before imaging to attain a density of 100,000 cells/well. The cells were treated with 100 ng/mL of ultrapure LPS for 4 h, after which they were incubated with LNPs/corona complexes as previously discussed for 12 h. Nigericin (1 $\mu$L/mL) was used as a positive control for ASC speck imaging. It was added to the wells 2 h before imaging. After LNPs/corona treatment, the cells were stained with propidium iodide (PI) stain (2 $\mu$g/mL) and NucBlue (2 drops/mL) and incubated at 37 °C. After 15 min of incubation, the cells were ready for imaging using the Crest V2 TIRF Spinning Disk Confocal Microscope.

**Flow Cytometry for Internalization.** Lipid nanoparticles were synthesized with 3 mol % of DiD dye to study the cellular uptake of LNPs/corona in macrophages. iBMDMs were first stained with 2 $\mu$M CFSE per the manufacturer's protocol and then seeded in a 12-well plate to reach a density of 1,000,000 cells per well. DiD encapsulating LNPs/corona were then added to the cells at 200 $\mu$g/mL concentration and incubated for 2 h. The cells were then removed and collected in 1 mL of 1× PBS using a cell scraper. The collected samples were centrifuged at 1500 rpm for 5 min and resuspended in 100 $\mu$L of 1× PBS. The samples were vortexed for mixing and then analyzed using the NovoExpress Software. Double-positive events were counted to estimate the extent of internalization.

**Light Microscopy for Lysosomal Rupture.** For studying lysosomal rupture, iBMDMs were seeded to achieve a density of 100,000 cells per well. As discussed before, LPS priming was done at the desired cell population for 2 h. Then, 0.3 mol % DiD encapsulated LNPs/corona were added to the cells for 4 h. After particle incubation, the cells were stained with NucBlue (2 drops/mL) and Lysotracker Red DnD-99 (0.1 $\mu$M) for 30 min. The cells were then imaged using a Nikon Crest V2 Spinning Disk Confocal Microscope. The analysis of the images was done using the NIS Elements software, and the graph was plotted in the Graph Pad Prism software. The lysosomal rupture was measured after normalizing with the number of LNPs that were taken up by the iBMDMs.

**Intracellular Calcium Influx and Mitochondrial ROS Detection.** To quantify calcium influx and mitochondrial ROS, iBMDMs were plated to achieve a population density of 100,000 cells per well of a 12-well plate. The cells were then primed with LPS for 2 h followed by particle/corona treatment for 4 h. The primed cells were treated with nigericin 1 h before the staining for positive control. After particle incubation, the cells were washed with PBS and stained with 1 $\mu$M Fluo-4 AM (acetoxymethyl) in CPBS at 37 °C for 30 min. They were then stained with 1 $\mu$M MitoSOX in HBSS at 37 °C for 20 min. After staining, cells were washed with PBS/HBSS, dislodged from the plate using a cell scraper, and centrifuged at 1500 rpm for 5 min to obtain the pellet. The cell pellets of different treatment groups were dissolved in PBS and quantified using the ACEA Novocyte flow cytometer.

**Corona Protein Quantification.** Protein quantification was done by using a Pierce BCA Protein Assay Kit. First, the corona complexes were formed by adding lipids and serum proteins in the ratio of 1:5 w/w. To quantify the proteins absorbed in the surface of the LNPs, we first removed all the unbound proteins, as discussed before, by ultracentrifuging the corona at 15,000$g$ for 15 min followed by washing with 1× PBS. Once the hard corona was achieved, we added the same volume containing a mixture of 1× PBS and the working reagent (as mentioned in the manufacturer's protocol) in a 1:8 v/v ratio and incubated it at 37 °C for 30 min. Then, the samples were centrifuged again at 15,000$g$ rpm for 15 min, and the supernatant was added in a 96-well plate along the BCA standards prepared before. The absorbance at 562 nm was measured in a microplate reader to quantify the proteins absorbed in the LNPs surface. For the SDS page, the proteins were eluted from the hard corona first before running the gel.

**LC−MS/MS Analysis.** As explained before, the nanoparticle−corona complexes were first ultracentrifuged and washed with PBS. To the pellet of the hard corona, we add 8 M urea, 100 mM ammonium bicarbonate, and 10 mM DTT for 30 min in a way that the final volume adds to the initial total volume. Iodoacetamide was then added at a concentration of 35 mM to alkylate the samples. Thirty minutes after adding the iodoacetamide, we added DTT to a final concentration of 35 mM to stop the alkylation. The samples were then diluted 5× with milli-Q, and then 1/30 w/w trypsin was added and kept at 37 °C overnight. The next morning, we ultracentrifuged the samples again to pellet down the LNPs, and the supernatants were collected for LC−MS analysis. Peptides were then separated by reverse-phase chromatography using nano-flow EASY-nLC 1000 UHPLC coupled to an Orbitrap Fusion mass spectrometer (Thermo Scientific) with a PepMap RSLCnano column (75 $\mu$m ID, 15 cm). Peptides were eluted over a 90 min 5−35% ACN gradient at 300 nL/min. Survey scans were measured in the Orbitrap analyzer at 60,000 resolutions. Data-dependent MS/MS data were collected in the linear ion trap using a 2 s cycle time with a full MS mass range from 400 to 1800 $m/z$. Peptides (charge states 2−6) were fragmented using higher-energy collisional dissociation using a normalized collision energy setting of 27. A dynamic exclusion time of 5 s was used, and the peptide match setting was enabled. RAW files were analyzed in Proteome Discoverer 2.4 (Thermo Scientific) using the SEQUEST search algorithm against the *Rattus norvegicus* (SwissProt TaxID = 10116) database downloaded from uniprot.org. The search parameters used are as follows: 10 ppm precursor ion tolerance and 0.4 Da fragment ion tolerance; up to two missed cleavages were allowed; dynamic modifications of methionine oxidation and N-terminal acetylation. Peptide matches were filtered to a protein false discovery rate of 5% using the Percolator algorithm. Peptides were assembled into proteins using maximum parsimony, and


https://doi.org/10.1021/acs.bioconjchem.3c00329
Bioconjugate Chem. 2023, 34, 1766−1779

only unique and razor peptides were retained for subsequent analysis.

**Inhibitor Study for Cellular Uptake Mechanism.** First, we figured out the minimum concentration of DiD that showed positive for internalization using flow cytometry. For that, we made LNPs with different concentrations of encapsulating DiD dye. DiD (0.03, 0.3, and 3%) containing LNPs/corona complexes were added to the iBMDMs for 2 h at the same lipid concentrations. The cells were then scraped off and centrifuged at 1500 rpm for 5 min and resuspended in 100 $\mu$L of 1× PBS containing 2% (v/v) of CD45 antibody. The samples were kept at 4 °C for 30 min and then dissolved in 1× PBS for flow cytometry. Double positives for CD45 and DiD were chosen to optimize the concentration of DiD dye.

For the experiments with inhibitors to study the cellular uptake, iBMDMs were treated with different pharmacological inhibitors to observe the cellular uptake of protein corona formed on two LNP systems. Here, iBMDMs were plated on a 12-well plate to achieve a density of 1,000,000 cells per well. At the desired cell population, the inhibitors were added to the cells at different concentrations for 2 h. The concentrations of inhibitors used in this study are 100 $\mu$m EIPA, 10 $\mu$m/mL chlorpromazine, 25 $\mu$m/mL Dynasore, 2.5 $\mu$m/mL cytochalasin D, and 5 $\mu$m nocodazole. LNPs/corona with 0.3% DiD dye were then added to the cells along with the same inhibitors for 2 h at a final lipid concentration of 200 $\mu$g/mL. LNPs were also added to the cells without any inhibitors to design a comparative study. After 2 h, the wells were scraped off with cell scrapers, and the collected samples were centrifuged and stained with CD45 (2% v/v) as discussed before. Following that, the samples were again centrifuged and resuspended in 1× PBS. They were then vortexed, and the double positives for DiD and CD45 were measured using the ACEA Novocyte flow cytometer. Graphs were plotted in GraphPad.

## ■ ASSOCIATED CONTENT

### Supporting Information

The Supporting Information is available free of charge at https://pubs.acs.org/doi/10.1021/acs.bioconjchem.3c00329.

> Pie chart representing the protein percentages of the 20 most abundant proteins (Figure S1); representative flow cytometry histogram and median fluorescence intensity (Figures S2 and S3); representative fractions and protein quantification (Figure S4); zeta potential characterization (Figure S5); involvement of the NLRP3 inflammasome in IL-1$\beta$ release (Figure S6); representative fluorescence microscopy imaging (Figure S7); LNP internalization (Figure S8); Pearson coefficient (Figure S9); and percentage of internalized in iBMDMs (Figure S10) (PDF)

## ■ AUTHOR INFORMATION


### Corresponding Author

**Ashish Kulkarni** − *Department of Chemical Engineering, University of Massachusetts Amherst, Amherst, Massachusetts 01003, United States; Department of Biomedical Engineering and Center for Bioactive Delivery, Institute for Applied Life Sciences, University of Massachusetts Amherst, Amherst, Massachusetts 01003, United States;* orcid.org/0000-0002-5713-2202; Email: akulkarni@engin.umass.edu

### Authors

**Maharshi Debnath** − *Department of Chemical Engineering, University of Massachusetts Amherst, Amherst, Massachusetts 01003, United States*

**James Forster, III** − *Department of Chemical Engineering, University of Massachusetts Amherst, Amherst, Massachusetts 01003, United States*

**Anujan Ramesh** − *Department of Biomedical Engineering, University of Massachusetts Amherst, Amherst, Massachusetts 01003, United States;* orcid.org/0000-0002-0173-5434

Complete contact information is available at: https://pubs.acs.org/10.1021/acs.bioconjchem.3c00329


### Author Contributions

The manuscript was written through the contributions of all authors, and all authors have approved the final version of the manuscript.

### Notes

The authors declare no competing financial interest.

## ■ ACKNOWLEDGMENTS

This work was financially supported by the National Science Foundation CAREER Award (2142917) to A. K. We would like to thank the Biophysical Characterization Core at the Institute for Applied Life Sciences (IALS), the University of Massachusetts Amherst, for lending their expertise in regard to characterization experiments. We would also like to thank the Light Microscopy Core Facility at the University of Massachusetts Amherst for their help and consultation while performing confocal imaging.

## ■ REFERENCES


(1) Tenchov, R.; Bird, R.; Curtze, A. E.; Zhou, Q. Lipid Nanoparticles═From Liposomes to MRNA Vaccine Delivery, a Landscape of Research Diversity and Advancement. *ACS Nano* **2021**, *15*, 16982−17015.

(2) Miller, A. D. Lipid-Based Nanoparticles in Cancer Diagnosis and Therapy. *J. Drug Delivery* **2013**, *2013*, No. 165981.

(3) Hou, X.; Zaks, T.; Langer, R.; Dong, Y. Lipid Nanoparticles for MRNA Delivery. *Nat. Rev. Mater.* **2021**, *6*, 1078−1094.

(4) Adeel, M.; Duzagac, F.; Canzonieri, V.; Rizzolio, F. Self-Therapeutic Nanomaterials for Cancer Therapy: A Review. *ACS Appl. Nano Mater.* **2020**, *3*, 4962−4971.

(5) Xu, L.; Wang, X.; Liu, Y.; Yang, G.; Falconer, R. J.; Zhao, C.-X. Lipid Nanoparticles for Drug Delivery. *Adv. Nano Biomed Res.* **2022**, *2*, 2100109.

(6) Ramachandran, S.; Satapathy, S. R.; Dutta, T. Delivery Strategies for MRNA Vaccines. *Pharm. Med.* **2022**, *36*, 11−20.

(7) Kiaie, S. H.; Majidi Zolbanin, N.; Ahmadi, A.; Bagherifar, R.; Valizadeh, H.; Kashanchi, F.; Jafari, R. Recent Advances in MRNA-LNP Therapeutics: Immunological and Pharmacological Aspects. *J. Nanobiotechnology* **2022**, *20*, 276.

(8) Battaglia, L.; Gallarate, M. Lipid Nanoparticles: State of the Art, New Preparation Methods and Challenges in Drug Delivery. *Expert Opin. Drug Deliv.* **2012**, *9*, 497−508.

(9) Rampado, R.; Crotti, S.; Caliceti, P.; Pucciarelli, S.; Agostini, M. Recent Advances in Understanding the Protein Corona of Nanoparticles and in the Formulation of "Stealthy" Nanomaterials. *Front. Bioeng. Biotechnol.* **2020**, *8*, 166.

(10) Rosenblum, D.; Joshi, N.; Tao, W.; Karp, J. M.; Peer, D. Progress and Challenges towards Targeted Delivery of Cancer Therapeutics. *Nat. Commun.* **2018**, *9*, 1410.

(11) Ventola, C. L. Progress in Nanomedicine: Approved and Investigational Nanodrugs. *Pharm. Ther.* **2017**, *42*, 742−755.

(12) Panico, S.; Capolla, S.; Bozzer, S.; Toffoli, G.; Dal Bo, M.; Macor, P. Biological Features of Nanoparticles: Protein Corona Formation and Interaction with the Immune System. *Pharmaceutics* **2022**, *14*, 2605.
(13) Walkey, C. D.; Chan, W. C. W. Understanding and Controlling the Interaction of Nanomaterials with Proteins in a Physiological Environment. *Chem. Soc. Rev.* **2012**, *41*, 2780−2799.
(14) Yu, Q.; Zhao, L.; Guo, C.; Yan, B.; Su, G. Regulating Protein Corona Formation and Dynamic Protein Exchange by Controlling Nanoparticle Hydrophobicity. *Front. Bioeng. Biotechnol.* **2020**, *8*, 210.
(15) García-Álvarez, R.; Vallet-Regí, M. Hard and Soft Protein Corona of Nanomaterials: Analysis and Relevance. *Nanomaterials* **2021**, *11*, 888.
(16) Francia, V.; Yang, K.; Deville, S.; Reker-Smit, C.; Nelissen, I.; Salvati, A. Corona Composition Can Affect the Mechanisms Cells Use to Internalize Nanoparticles. *ACS Nano* **2019**, *13*, 11107−11121.
(17) Saptarshi, S. R.; Duschl, A.; Lopata, A. L. Interaction of Nanoparticles with Proteins: Relation to Bio-Reactivity of the Nanoparticle. *J. Nanobiotechnology* **2013**, *11*, 26.
(18) Oh, J. Y.; Kim, H. S.; Palanikumar, L.; Go, E. M.; Jana, B.; Park, S. A.; Kim, H. Y.; Kim, K.; Seo, J. K.; Kwak, S. K.; Kim, C.; Kang, S.; Ryu, J.-H. Cloaking Nanoparticles with Protein Corona Shield for Targeted Drug Delivery. *Nat. Commun.* **2018**, *9*, 4548.
(19) Akhter, M. H.; Khalilullah, H.; Gupta, M.; Alfaleh, M. A.; Alhakamy, N. A.; Riadi, Y.; Md, S. Impact of Protein Corona on the Biological Identity of Nanomedicine: Understanding the Fate of Nanomaterials in the Biological Milieu. *Biomedicines* **2021**, *9*, 1496.
(20) Walkey, C. D.; Olsen, J. B.; Guo, H.; Emili, A.; Chan, W. C. W. Nanoparticle Size and Surface Chemistry Determine Serum Protein Adsorption and Macrophage Uptake. *J. Am. Chem. Soc.* **2012**, *134*, 2139−2147.
(21) Park, J.-Y.; Park, S. J.; Park, J. Y.; Kim, S.-H.; Kwon, S.; Jung, Y.; Khang, D. Unfolded Protein Corona Surrounding Nanotubes Influence the Innate and Adaptive Immune System. *Adv. Sci.* **2021**, *8*, 2004979.
(22) Yang, H.; Lu, S.; Wang, S.; Liu, L.; Zhu, B.; Yu, S.; Yang, S.; Chang, J. Evolution of the Protein Corona Affects Macrophage Polarization. *Int. J. Biol. Macromol.* **2021**, *191*, 192−200.
(23) Pavlin, M.; Lojk, J.; Strojan, K.; Hafner-Bratkovič, I.; Jerala, R.; Leonardi, A.; Križaj, I.; Drnovšek, N.; Novak, S.; Veranič, P.; Bregar, V. B. The Relevance of Physico-Chemical Properties and Protein Corona for Evaluation of Nanoparticles Immunotoxicity-In Vitro Correlation Analysis on THP-1 Macrophages. *Int. J. Mol. Sci.* **2022**, *23*, 6197.
(24) Ma, X.; Li, Y.; Shen, W.; Oladejo, A. O.; Yang, J.; Jiang, W.; Imam, B. H.; Wu, X.; Ding, X.; Yang, Y.; Wang, S.; Yan, Z. LPS Mediates Bovine Endometrial Epithelial Cell Pyroptosis Directly Through Both NLRP3 Classical and Non-Classical Inflammasome Pathways. *Front. Immunol.* **2021**, *12*, No. 676088.
(25) Froster, J. Iii; Nandi, D.; Kulkarni, A. MRNA-Carrying Lipid Nanoparticles That Induce Lysosomal Rupture Activate NLRP3 Inflammasome and Reduce MRNA Transfection Efficiency. *Biomater. Sci.* **2022**, *10*, 5566−5582.
(26) Fusco, R.; Siracusa, R.; Genovese, T.; Cuzzocrea, S.; Di Paola, R. Focus on the Role of NLRP3 Inflammasome in Diseases. *Int. J. Mol. Sci.* **2020**, *21*, 4223.
(27) Kelley, N.; Jeltema, D.; Duan, Y.; He, Y. The NLRP3 Inflammasome: An Overview of Mechanisms of Activation and Regulation. *Int. J. Mol. Sci.* **2019**, *20*, 3328.
(28) *An update on the regulatory mechanisms of NLRP3 inflammasome activation | Cellular & Molecular Immunology*. https://www.nature.com/articles/s41423-021-00670-3 (accessed 2023-03-04).
(29) He, Y.; Hara, H.; Núñez, G. Mechanism and Regulation of NLRP3 Inflammasome Activation. *Trends Biochem. Sci.* **2016**, *41*, 1012−1021.
(30) Nandi, D.; Shivrayan, M.; Gao, J.; Krishna, J.; Das, R.; Liu, B.; Thayumanavan, S.; Kulkarni, A. Core Hydrophobicity of Supramolecular Nanoparticles Induces NLRP3 Inflammasome Activation. *ACS Appl. Mater. Interfaces* **2021**, *13*, 45300−45314.
(31) Baron, L.; Gombault, A.; Fanny, M.; Villeret, B.; Savigny, F.; Guillou, N.; Panek, C.; Le Bert, M.; Lagente, V.; Rassendren, F.; Riteau, N.; Couillin, I. The NLRP3 Inflammasome Is Activated by Nanoparticles through ATP, ADP and Adenosine. *Cell Death Dis.* **2015**, *6*, e1629−e1629.
(32) Gómez, D. M.; Urcuqui-Inchima, S.; Hernandez, J. C. Silica Nanoparticles Induce NLRP3 Inflammasome Activation in Human Primary Immune Cells. *Innate Immun.* **2017**, *23*, 697−708.
(33) Riley, R. S.; Kashyap, M. V.; Billingsley, M. M.; White, B.; Alameh, M.-G.; Bose, S. K.; Zoltick, P. W.; Li, H.; Zhang, R.; Cheng, A. Y.; Weissman, D.; Peranteau, W. H.; Mitchell, M. J. Ionizable Lipid Nanoparticles for in Utero MRNA Delivery. *Sci. Adv.* **2021**, *7*, No. eaba1028.
(34) Coelho, T.; Adams, D.; Silva, A.; Lozeron, P.; Hawkins, P. N.; Mant, T.; Perez, J.; Chiesa, J.; Warrington, S.; Tranter, E.; Munisamy, M.; Falzone, R.; Harrop, J.; Cehelsky, J.; Bettencourt, B. R.; Geissler, M.; Butler, J. S.; Sehgal, A.; Meyers, R. E.; Chen, Q.; Borland, T.; Hutabarat, R. M.; Clausen, V. A.; Alvarez, R.; Fitzgerald, K.; Gamba-Vitalo, C.; Nochur, S. V.; Vaishnaw, A. K.; Sah, D. W. Y.; Gollob, J. A.; Suhr, O. B. Safety and Efficacy of RNAi Therapy for Transthyretin Amyloidosis. *N. Engl. J. Med.* **2013**, *369*, 819−829.
(35) Joseph, R. R.; Tan, D. W. N.; Ramon, M. R. M.; Natarajan, J. V.; Agrawal, R.; Wong, T. T.; Venkatraman, S. S. Characterization of Liposomal Carriers for the Trans-Scleral Transport of Ranibizumab. *Sci. Rep.* **2017**, *7*, 16803.
(36) Zhong, Z.; Zhai, Y.; Liang, S.; Mori, Y.; Han, R.; Sutterwala, F. S.; Qiao, L. TRPM2 Links Oxidative Stress to NLRP3 Inflammasome Activation. *Nat. Commun.* **2013**, *4*, 1611.
(37) Silvius, J. R. Role of Cholesterol in Lipid Raft Formation: Lessons from Lipid Model Systems. *Biochim. Biophys. Acta BBA - Biomembr.* **2003**, *1610*, 174−183.
(38) Gräfe, C.; Weidner, A.; Lühe, M. V. D.; Bergemann, C.; Schacher, F. H.; Clement, J. H.; Dutz, S. Intentional Formation of a Protein Corona on Nanoparticles: Serum Concentration Affects Protein Corona Mass, Surface Charge, and Nanoparticle−Cell Interaction. *Int. J. Biochem. Cell Biol.* **2016**, *75*, 196−202.
(39) Barbero, F.; Russo, L.; Vitali, M.; Piella, J.; Salvo, I.; Borrajo, M. L.; Busquets-Fité, M.; Grandori, R.; Bastús, N. G.; Casals, E.; Puntes, V. Formation of the Protein Corona: The Interface between Nanoparticles and the Immune System. *Semin. Immunol.* **2017**, *34*, 52−60.
(40) Deutsch, E. W. File Formats Commonly Used in Mass Spectrometry Proteomics. *Mol. Cell. Proteomics* **2012**, *11*, 1612−1621.
(41) Cai, R.; Ren, J.; Guo, M.; Wei, T.; Liu, Y.; Xie, C.; Zhang, P.; Guo, Z.; Chetwynd, A. J.; Ke, P. C.; Lynch, I.; Chen, C. Dynamic Intracellular Exchange of Nanomaterials' Protein Corona Perturbs Proteostasis and Remodels Cell Metabolism. *Proc. Natl. Acad. Sci.* **2022**, *119*, No. e2200363119.
(42) Cullis, P. R.; Chonn, A.; Semple, S. C. Interactions of Liposomes and Lipid-Based Carrier Systems with Blood Proteins: Relation to Clearance Behaviour in Vivo. *Adv. Drug Delivery Rev.* **1998**, *32*, 3−17.
(43) Ngo, W.; Wu, J. L. Y.; Lin, Z. P.; Zhang, Y.; Bussin, B.; Granda Farias, A.; Syed, A. M.; Chan, K.; Habsid, A.; Moffat, J.; Chan, W. C. W. Identifying Cell Receptors for the Nanoparticle Protein Corona Using Genome Screens. *Nat. Chem. Biol.* **2022**, *18*, 1023−1031.
(44) Yan, Y.; Gause, K. T.; Kamphuis, M. M. J.; Ang, C.-S.; O'Brien-Simpson, N. M.; Lenzo, J. C.; Reynolds, E. C.; Nice, E. C.; Caruso, F. Differential Roles of the Protein Corona in the Cellular Uptake of Nanoporous Polymer Particles by Monocyte and Macrophage Cell Lines. *ACS Nano* **2013**, *7*, 10960−10970.
(45) Mohammad-Beigi, H.; Hayashi, Y.; Zeuthen, C. M.; Eskandari, H.; Scavenius, C.; Juul-Madsen, K.; Vorup-Jensen, T.; Enghild, J. J.; Sutherland, D. S. Mapping and Identification of Soft Corona Proteins at Nanoparticles and Their Impact on Cellular Association. *Nat. Commun.* **2020**, *11*, 4535.
(46) Nguyen, V. H.; Lee, B.-J. Protein Corona: A New Approach for Nanomedicine Design. *Int. J. Nanomed.* **2017**, *Volume 12*, 3137−3151.


https://doi.org/10.1021/acs.bioconjchem.3c00329
*Bioconjugate Chem.* 2023, 34, 1766−1779

(47) Mouasni, S.; Gonzalez, V.; Schmitt, A.; Bennana, E.; Guillonneau, F.; Mistou, S.; Avouac, J.; Ea, H. K.; Devauchelle, V.; Gottenberg, J.-E.; Chiocchia, G.; Tourneur, L. The Classical NLRP3 Inflammasome Controls FADD Unconventional Secretion through Microvesicle Shedding. *Cell Death Dis.* **2019**, *10*, 1−18.
(48) Pizzuto, M.; Bigey, P.; Lachagès, A.-M.; Hoffmann, C.; Ruysschaert, J.-M.; Escriou, V.; Lonez, C. Cationic Lipids as One-Component Vaccine Adjuvants: A Promising Alternative to Alum. *J. Control. Rel.* **2018**, *287*, 67−77.
(49) Lonez, C.; Bessodes, M.; Scherman, D.; Vandenbranden, M.; Escriou, V.; Ruysschaert, J.-M. Cationic Lipid Nanocarriers Activate Toll-like Receptor 2 and NLRP3 Inflammasome Pathways. *Nanomed. Nanotechnol. Biol. Med.* **2014**, *10*, 775−782.
(50) Corbo, C.; Molinaro, R.; Parodi, A.; Toledano Furman, N. E.; Salvatore, F.; Tasciotti, E. The Impact of Nanoparticle Protein Corona on Cytotoxicity, Immunotoxicity and Target Drug Delivery. *Nanomed.* **2016**, *11*, 81−100.
(51) Li, H.; Wang, Y.; Tang, Q.; Yin, D.; Tang, C.; He, E.; Zou, L.; Peng, Q. The Protein Corona and Its Effects on Nanoparticle-Based Drug Delivery Systems. *Acta Biomater.* **2021**, *129*, 57−72.
(52) Nagar, A.; Rahman, T.; Harton, J. A. The ASC Speck and NLRP3 Inflammasome Function Are Spatially and Temporally Distinct. *Front. Immunol.* **2021**, *12*, No. 752482.
(53) Compan, V.; Martín-Sánchez, F.; Baroja-Mazo, A.; López-Castejón, G.; Gomez, A. I.; Verkhratsky, A.; Brough, D.; Pelegrín, P. Apoptosis-Associated Speck-like Protein Containing a CARD Forms Specks but Does Not Activate Caspase-1 in the Absence of NLRP3 during Macrophage Swelling. *J. Immunol.* **2015**, *194*, 1261−1273.
(54) Katsnelson, M. A.; Lozada-Soto, K. M.; Russo, H. M.; Miller, B. A.; Dubyak, G. R. NLRP3 Inflammasome Signaling Is Activated by Low-Level Lysosome Disruption but Inhibited by Extensive Lysosome Disruption: Roles for K+ Efflux and Ca2+ Influx. *Am. J. Physiol.-Cell Physiol* **2016**, *311*, C83−C100.
(55) Nandi, D.; Farid, N. S. S.; Karuppiah, H. A. R.; Kulkarni, A. Imaging Approaches to Monitor Inflammasome Activation. *J. Mol. Biol.* **2022**, *434*, No. 167251.
(56) Tenzer, S.; Docter, D.; Kuharev, J.; Musyanovych, A.; Fetz, V.; Hecht, R.; Schlenk, F.; Fischer, D.; Kiouptsi, K.; Reinhardt, C.; Landfester, K.; Schild, H.; Maskos, M.; Knauer, S. K.; Stauber, R. H. Rapid Formation of Plasma Protein Corona Critically Affects Nanoparticle Pathophysiology. *Nat. Nanotechnol.* **2013**, *8*, 772−781.
(57) Barrán-Berdón, A. L.; Pozzi, D.; Caracciolo, G.; Capriotti, A. L.; Caruso, G.; Cavaliere, C.; Riccioli, A.; Palchetti, S.; Laganà, A. Time Evolution of Nanoparticle-Protein Corona in Human Plasma: Relevance for Targeted Drug Delivery. *Langmuir ACS J. Surf. Colloids* **2013**, *29*, 6485−6494.
(58) Mazzolini, J.; Weber, R. J. M.; Chen, H.-S.; Khan, A.; Guggenheim, E.; Shaw, R. K.; Chipman, J. K.; Viant, M. R.; Rappoport, J. Z. Protein Corona Modulates Uptake and Toxicity of Nanoceria via Clathrin-Mediated Endocytosis. *Biol. Bull.* **2016**, *231*, 40−60.
(59) Vu, V. P.; Gifford, G. B.; Chen, F.; Benasutti, H.; Wang, G.; Groman, E. V.; Scheinman, R.; Saba, L.; Moghimi, S. M.; Simberg, D. Immunoglobulin Deposition on Biomolecule Corona Determines Complement Opsonization Efficiency of Preclinical and Clinical Nanoparticles. *Nat. Nanotechnol.* **2019**, *14*, 260−268.
(60) Lu, F.; Sun, J.; Sun, T.; Cheng, H.; Yang, S. Fluorescence-Based Measurements of Store-Operated Ca2+ Entry in Cancer Cells Using Fluo-4 and Confocal Live Cell Imaging. *Methods Mol. Biol. Clifton NJ* **2018**, *2018*, 63−68.
(61) Kauffman, M.; Kauffman, M.; Traore, K.; Zhu, H.; Trush, M.; Jia, Z.; Li, Y. R. MitoSOX-Based Flow Cytometry for Detecting Mitochondrial ROS. *React. Oxyg. Species Apex NC* **2016**, *2*, 361−370.
(62) Lima, H., Jr.; Jacobson, L. S.; Goldberg, M. F.; Chandran, K.; Diaz-Griffero, F.; Lisanti, M. P.; Brojatsch, J. Role of Lysosome Rupture in Controlling Nlrp3 Signaling and Necrotic Cell Death. *Cell Cycle* **2013**, *12*, 1868−1878.
(63) Seoane, P. I.; Lee, B.; Hoyle, C.; Yu, S.; Lopez-Castejon, G.; Lowe, M.; Brough, D. The NLRP3−Inflammasome as a Sensor of Organelle Dysfunction. *J. Cell Biol.* **2020**, *219*, No. e202006194.
(64) Yang, Y.; Wang, H.; Kouadir, M.; Song, H.; Shi, F. Recent Advances in the Mechanisms of NLRP3 Inflammasome Activation and Its Inhibitors. *Cell Death Dis.* **2019**, *10*, 1−11.
(65) Chazotte, B. Labeling Lysosomes in Live Cells with LysoTracker. *Cold Spring Harb. Protoc.* **2011**, *2011*, No. pdb.prot5571.
(66) Janeway, J.; Travers, P.; Walport, M.; Shlomchik, M. J. The Front Line of Host Defense. *Immunobiol. Immune Syst. Health Dis. 5th Ed.*Garland Science 2001.
(67) Leseigneur, C.; Lê-Bury, P.; Pizarro-Cerdá, J.; Dussurget, O. Emerging Evasion Mechanisms of Macrophage Defenses by Pathogenic Bacteria. *Front. Cell. Infect. Microbiol.* **2020**, *10*, No. 577559.
(68) Aderem, A.; Underhill, D. M. Mechanisms of Phagocytosis in Macrophages. *Annu. Rev. Immunol.* **1999**, *17*, 593−623.
(69) Caracciolo, G.; Palchetti, S.; Colapicchioni, V.; Digiacomo, L.; Pozzi, D.; Capriotti, A. L.; La Barbera, G.; Laganà, A. Stealth Effect of Biomolecular Corona on Nanoparticle Uptake by Immune Cells. *Langmuir* **2015**, *31*, 10764−10773.
(70) Rejman, J.; Oberle, V.; Zuhorn, I. S.; Hoekstra, D. Size-Dependent Internalization of Particles via the Pathways of Clathrin- and Caveolae-Mediated Endocytosis. *Biochem. J.* **2004**, *377*, 159−169.
(71) Kovtun, O.; Dickson, V. K.; Kelly, B. T.; Owen, D. J.; Briggs, J. A. G. Architecture of the AP2/Clathrin Coat on the Membranes of Clathrin-Coated Vesicles. *Sci. Adv.* **2020**, *6*, No. eaba8381.
(72) Vercauteren, D.; Vandenbroucke, R. E.; Jones, A. T.; Rejman, J.; Demeester, J.; De Smedt, S. C.; Sanders, N. N.; Braeckmans, K. The Use of Inhibitors to Study Endocytic Pathways of Gene Carriers: Optimization and Pitfalls. *Mol. Ther.* **2010**, *18*, 561−569.
(73) Bouley, R.; Yui, N.; Terlouw, A.; Cheung, P. W.; Brown, D. Chlorpromazine Induces Basolateral Aquaporin-2 Accumulation via F-Actin Depolymerization and Blockade of Endocytosis in Renal Epithelial Cells. *Cells* **2020**, *9*, 1057.
(74) Preta, G.; Cronin, J. G.; Sheldon, I. M. Dynasore - Not Just a Dynamin Inhibitor. *Cell Commun. Signal.* **2015**, *13*, 24.
(75) Koivusalo, M.; Welch, C.; Hayashi, H.; Scott, C. C.; Kim, M.; Alexander, T.; Touret, N.; Hahn, K. M.; Grinstein, S. Amiloride Inhibits Macropinocytosis by Lowering Submembranous PH and Preventing Rac1 and Cdc42 Signaling. *J. Cell Biol.* **2010**, *188*, 547−563.
(76) Casella, J. F.; Flanagan, M. D.; Lin, S. Cytochalasin D Inhibits Actin Polymerization and Induces Depolymerization of Actin Filaments Formed during Platelet Shape Change. *Nature* **1981**, *293*, 302−305.
(77) Moghimi, S. M.; Simberg, D. Pro-Inflammatory Concerns with Lipid Nanoparticles. *Mol. Ther.* **2022**, *30*, 2109−2110.
(78) Han, S.; da Costa Marques, R.; Simon, J.; Kaltbeitzel, A.; Koynov, K.; Landfester, K.; Mailänder, V.; Lieberwirth, I. Endosomal Sorting Results in a Selective Separation of the Protein Corona from Nanoparticles. *Nat. Commun.* **2023**, *14*, 295.
(79) Salvati, A.; Pitek, A. S.; Monopoli, M. P.; Prapainop, K.; Bombelli, F. B.; Hristov, D. R.; Kelly, P. M.; Åberg, C.; Mahon, E.; Dawson, K. A. Transferrin-Functionalized Nanoparticles Lose Their Targeting Capabilities When a Biomolecule Corona Adsorbs on the Surface. *Nat. Nanotechnol.* **2013**, *8*, 137−143.
(80) Lara, S.; Alnasser, F.; Polo, E.; Garry, D.; Lo Giudice, M. C.; Hristov, D. R.; Rocks, L.; Salvati, A.; Yan, Y.; Dawson, K. A. Identification of Receptor Binding to the Biomolecular Corona of Nanoparticles. *ACS Nano* **2017**, *11*, 1884−1893.


https://doi.org/10.1021/acs.bioconjchem.3c00329
*Bioconjugate Chem.* 2023, 34, 1766−1779